

MULTICHANNEL OPTICAL APERTURE SYNTHESIS IMAGING OF  $\zeta^1$  URSAE MAJORIS  
WITH THE NAVY PROTOTYPE OPTICAL INTERFEROMETER

J. A. BENSON,<sup>1</sup> D. J. HUTTER, N. M. ELIAS II,<sup>1</sup> P. F. BOWERS,<sup>1</sup> K. J. JOHNSTON, AND A. R. HAJIAN

U.S. Naval Observatory, 3450 Massachusetts Avenue NW, Washington, DC 20392-5420

Electronic mail: jbenso@nofs.navy.mil, djh@fornax.usno.navy.mil, nme@sextans.lowell.edu, kjj@astro.usno.navy.mil,  
hajian@fornax.usno.navy.mil

J. T. ARMSTRONG,<sup>2</sup> D. MOZURKEWICH, T. A. PAULS, AND L. J. RICKARD

Remote Sensing Division, Naval Research Laboratory, Code 7210, Washington, DC 20375

Electronic mail: tarmstr@fornax.usno.navy.mil, mozurk@rira.nrl.navy.mil, pauls@atlas.nrl.navy.mil, rickard@rira.nrl.navy.mil

C. A. HUMMEL<sup>2</sup>

Universities Space Research Association, 300 D Street SW, Washington, DC 20024

Electronic mail: cah@fornax.usno.navy.mil

N. M. WHITE, D. BLACK, AND C. S. DENISON

Lowell Observatory, 1400 W. Mars Hill Road, Flagstaff, Arizona 86001

Electronic mail: nmw@lowell.edu, cdenison@sextans.lowell.edu

Received 1997 April 7; revised 1997 June 2

ABSTRACT

We have used the Navy Prototype Optical Interferometer (NPOI) to obtain the first multichannel optical aperture synthesis images of a star. We observed the spectroscopic binary  $\zeta^1$  Ursae Majoris at 6 to 10 milliarcseconds separation during seven nights, using three interferometric baselines and 19 spectral channels ( $\lambda\lambda$  520–850 nm) of the NPOI. After editing, a typical 90 sec scan yielded fringe visibilities at 50 spatial frequencies and closure phases at 15 wavelengths. Three to five scans were obtained each night. The separations and position angles are in good agreement with the visual orbit obtained with the Mark III interferometer (Hummel *et al.* 1995, AJ, 110, 376) but show small systematic difference that can be used to improve the orbit. The closure phase data provide a sensitive measure of the magnitude difference between the components. These results demonstrate the power of broad-band interferometric observations for fast imaging and the utility of vacuum delay lines for simultaneous observations over a wide band. These observations are the first to produce simultaneous visibilities and closure phases with a separate-aperture optical interferometer, and the second to produce closure phase images, following the results from COAST reported by Baldwin *et al.* (1996, A&A, 306, L13). The angular resolution here is the highest ever achieved at visual wavelengths, exceeding by an order of magnitude the best thus far achieved by any single-aperture optical telescope. We generated complex visibilities and closure phases (the data types commonly used in radio interferometry) from the optical data and used standard radio interferometry techniques to produce these images. However, the fundamental observables of optical interferometry, the squared visibility amplitude and the closure phase, require the development of new analysis techniques. © 1997 American Astronomical Society. [S0004-6256(97)01709-3]

1. INTRODUCTION

Atmospheric turbulence limited the resolution of telescopes at visual wavelengths until early in the twentieth century, when A. A. Michelson demonstrated that interferometry had the potential of measuring the exceedingly small angular diameters of stars (Michelson & Pease 1921). Michelson also realized that measurements of fringe visibilities

could be used to image stellar surfaces. The use of interferometry to measure orbits of binary stars also began early in this century (Anderson 1920). Brown *et al.* (1974) used intensity interferometry to measure stellar angular diameters. Speckle interferometry, a somewhat different technique, has also been used to measure binary orbits.

Atmospheric turbulence limits interferometry as well, by rapidly shifting the interference fringes. After Johnson *et al.* (1974) and Labeyrie (1975) showed that the fringe amplitude can be measured with an interferometer consisting of mechanically separate telescopes, Shao & Staelin (1977) demonstrated that, with computer-controlled delay lines and high-speed detectors, the optical fringe phase can be stabi-

<sup>1</sup>Mailing address: U.S. Naval Observatory Flagstaff Station, P.O. Box 1149, Flagstaff, AZ 86002-1149.

<sup>2</sup>Mailing address: NRL/USNO Optical Interferometer Project, Astrometry Division AD-5, US Naval Observatory, 3450 Massachusetts Avenue NW, Washington, DC 20392.

# Report Documentation Page

*Form Approved*  
*OMB No. 0704-0188*

Public reporting burden for the collection of information is estimated to average 1 hour per response, including the time for reviewing instructions, searching existing data sources, gathering and maintaining the data needed, and completing and reviewing the collection of information. Send comments regarding this burden estimate or any other aspect of this collection of information, including suggestions for reducing this burden, to Washington Headquarters Services, Directorate for Information Operations and Reports, 1215 Jefferson Davis Highway, Suite 1204, Arlington VA 22202-4302. Respondents should be aware that notwithstanding any other provision of law, no person shall be subject to a penalty for failing to comply with a collection of information if it does not display a currently valid OMB control number.

1. REPORT DATE <b>SEP 1997</b>	2. REPORT TYPE	3. DATES COVERED <b>00-00-1997 to 00-00-1997</b>			
4. TITLE AND SUBTITLE <b>Multichannel Optical Aperture Synthesis Imaging Of zeta1 URSAE Majoris With The Navy Prototype Optical Interferometer</b>		5a. CONTRACT NUMBER			
		5b. GRANT NUMBER			
		5c. PROGRAM ELEMENT NUMBER			
6. AUTHOR(S)		5d. PROJECT NUMBER			
		5e. TASK NUMBER			
		5f. WORK UNIT NUMBER			
7. PERFORMING ORGANIZATION NAME(S) AND ADDRESS(ES) <b>U. S. Naval Observatory, 3450 Massachusetts Ave, NW, Washington, DC, 20392</b>		8. PERFORMING ORGANIZATION REPORT NUMBER			
9. SPONSORING/MONITORING AGENCY NAME(S) AND ADDRESS(ES)		10. SPONSOR/MONITOR'S ACRONYM(S)			
		11. SPONSOR/MONITOR'S REPORT NUMBER(S)			
12. DISTRIBUTION/AVAILABILITY STATEMENT <b>Approved for public release; distribution unlimited</b>					
13. SUPPLEMENTARY NOTES <b>The Astronomical Journal, Vol 114, Number 3, September 1997</b>					
14. ABSTRACT					
15. SUBJECT TERMS					
16. SECURITY CLASSIFICATION OF:			17. LIMITATION OF ABSTRACT <b>Same as Report (SAR)</b>	18. NUMBER OF PAGES <b>7</b>	19a. NAME OF RESPONSIBLE PERSON
a. REPORT <b>unclassified</b>	b. ABSTRACT <b>unclassified</b>	c. THIS PAGE <b>unclassified</b>			

lized and tracked for hours. The Mark III optical interferometer on Mt. Wilson (Shao *et al.* 1988) advanced this technology and demonstrated the capabilities of a two-element interferometer for measuring stellar diameters (e.g., Hutter *et al.* 1989; Mozurkewich *et al.* 1991, 1997) and positions (e.g., Hummel *et al.* 1994), as well as binary orbits (e.g., Hummel *et al.* 1995).

The next step in optical interferometry is the extension to multiple baselines, to which the phase-closure techniques first espoused by Jennison (1958) and subsequently developed for very long baseline radio interferometry (VLBI) can be applied. In general, closure phase is needed to obtain unambiguous images from an interferometer. A two-dimensional multibaseline array with baseline lengths of 100 m or more could image stars with sub-milliarcsecond resolution. This paper describes a significant milestone achieved in the construction of such an array, the Navy Prototype Optical Interferometer (NPOI), a joint project of the US Naval Research Laboratory and the US Naval Observatory in cooperation with Lowell Observatory.

We report the first images obtained with the NPOI, made with simultaneous multichannel closure phase and visibility amplitude data. We observed the spectroscopic binary  $\zeta^1$  Ursae Majoris [Mizar A,  $m_V=2.27$ ,  $P=20^d.54$ ,  $a=9.64$  milliarcseconds (mas) (Hummel *et al.* 1995)] on seven nights between 1996 May 1 and June 4. Processing our closure phases and visibility amplitudes with standard interferometric image synthesis techniques, we have achieved a spatial resolution of  $\approx 3$  mas. Our achieved resolution exceeds by factors of two to three the best resolution *theoretically* obtainable by the current generation of monolithic optical telescopes. The closure phases produce a sensitive measure of the brightness ratio of the two components. We show here that, by taking data simultaneously in multiple spectral channels (in these images, we use 19 channels spanning a factor of 1.6 in spatial frequency), we greatly increase the speed with which images can be made.

The observations described here produced only the second closure phase measurements ever made with a separate-element optical interferometer. They are the first observations with simultaneous closure phase and visibility amplitude measurements, and the first with multibaseline data taken in more than one spectral channel. The first closure-phase measurements, in observations of the 56 mas binary  $\alpha$  Aurigae (Capella), were reported by the COAST group at Cambridge University (Baldwin *et al.* 1996).

## 2. THE NPOI

The NPOI, located at the Lowell Observatory site on Anderson Mesa, near Flagstaff, Arizona, is a long-baseline optical interferometer which will consist of an astrometric sub-array (four elements) and an imaging sub-array (six elements) when construction is complete (Armstrong *et al.* 1997). The purpose of the NPOI is to determine the precise positions of bright stars and to image the surfaces and circumstellar environments of nearby stars and stellar systems. The array elements are 50 cm siderostats; however, only 12.5 cm of the aperture is currently used, a limit set by the size of

the feed system optics. Beam-compressing telescopes, which will increase the useable apertures to 35 cm, are currently being built for the astrometric sub-array.

The NPOI uses 32 spectral channels covering a wide band ( $\lambda\lambda$  450–850 nm) to increase its sensitivity and its range of spatial frequencies, and to help determine the effect of atmospheric longitudinal dispersion on the fringe positions. Each channel corresponds to a spatial frequency of  $D/\lambda$ , where  $D$  is the baseline length and  $\lambda$  is the mean wavelength. In addition, the NPOI uses vacuum delay lines to ensure that fringes over the entire band can be observed simultaneously. Without vacuum delay lines, the large differences in air path length between the individual light paths and the variation in the index of refraction of air over the visual range produce a large variation of fringe phase with wavelength, precluding broadband observations that extend into the blue part of the visual spectrum. The instrument incorporates active group-delay fringe tracking and rapid tip-tilt star tracking. Avalanche photodiodes are used in both the fringe detection and star tracking systems.

The first single-baseline stellar fringe measurements at the NPOI were obtained in 1994 October. After numerous equipment, infrastructure, and software upgrades, including the addition of the third siderostat, the first three-baseline stellar fringe observations, including closure-phase measurements, were made on 1996 March 18.

As with the Mark III interferometer, the NPOI modulates the delay on each baseline by a small number of wavelengths and, for each spectral channel and baseline, synchronously measures the photon count rates in  $n$  bins per wavelength of modulation. (Currently,  $n=8$  for the NPOI; for the Mark III,  $n=4$ .) We generate the complex Fourier transform of this set of bins and select the component corresponding to a frequency of one fringe per  $n$  bins. The real and imaginary parts of this component are  $X$  and  $Y$ , respectively. The unbiased estimator for the squared visibility amplitude  $V^2$  for one baseline is given by

$$V^2 = \left[ \frac{4}{\text{sinc}^2(1/n)} \right] \frac{\langle X^2 + Y^2 - \sigma_N^2 \rangle}{\langle N \rangle^2}. \quad (1)$$

Here,  $N$  is the total number of photons in a frame of  $n$  bins, and  $\text{sinc}(x) \equiv \sin(\pi x)/\pi x$ . Subtracting  $\sigma_N^2$ , the variance of  $N$ , from  $X^2 + Y^2$  corrects for the bias due to noise (see Tango & Twiss 1980, who treat the case of shot noise, in which  $\sigma_N = N$ ). We calculate  $V^2$  rather than  $|V|$  because the bias correction for  $|V|$  depends on the value of  $|V|$  itself. The numerator and denominator are computed separately for every 2 ms sample interval and averaged for 1 s. The 1 s records are edited and further averaged over the length of the scan. The complex Fourier components  $X+iY$  from the three baselines are multiplied together every 2 ms to give the complex triple product. We average the triple product coherently, since the atmospheric phase noise cancels. The phase of the triple product is the closure phase,  $\phi_{cl}$ .

The calibration of the observed average  $V^2$  and  $\phi_{cl}$  is based on unresolved single stars. For unresolved sources, the theoretical  $V^2$  and  $\phi_{cl}$  are one and zero, respectively. The deviations of the measured  $V^2$  and  $\phi_{cl}$  of the unresolved calibrators from these values can be written as low-order

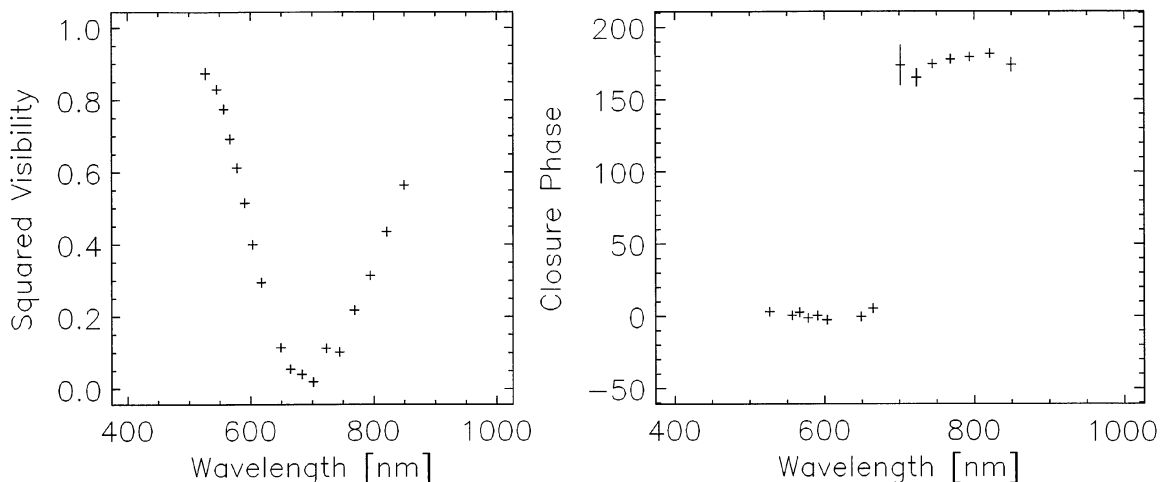


FIG. 1. Squared visibility amplitude,  $V^2$ , and closure phase,  $\phi_{cl}$ , vs wavelength for the first scan of 1996 May 1. The  $V^2$  shown are from the spectrometer for the EW baseline; data from bad detectors and from the channel contaminated by scattered HeNe laser metrology light were deleted. The closure phase combines data from all three spectrometers, one per baseline. A bad channel in any spectrometer precludes measuring  $\phi_{cl}$  at that wavelength; thus more channels are missing from these data than from the EW  $V^2$  data. For both  $V^2$  and  $\phi_{cl}$ , wavelengths shortward of  $\lambda 520$  nm were deleted because of low signal-to-noise ratio. The formal uncertainties in  $V^2$  are smaller than the symbols, but the calibration uncertainties are  $\sim \pm 10\%$ . For  $\phi_{cl}$ , the formal uncertainties are again smaller than the symbols, but the calibration uncertainties are  $\sim \pm 2^\circ$ .

polynomial functions of atmospheric and instrumental variables. The polynomial coefficients are determined from the calibrator scans and subsequently applied to the data of both the program sources and the calibrators. The deviation between the calibrated data of the calibrator stars and their expected values is a measure of the accuracy of our calibration procedure.

### 3. THE DATA AND RESULTING IMAGES

We used the center (C), east (E), and west (W) siderostats of the astrometric sub-array to observe  $\zeta^1$  Ursae Majoris on 1996 May 1–4 and 29, and June 1 and 4. Several calibration stars were observed each night, including a nearby calibrator,  $\gamma$  UMa. The baseline lengths were 18.9, 22.2, and 37.5 m at azimuths  $-67^\circ.5$ ,  $63^\circ.6$ , and  $86^\circ.0$ , respectively. Between three and five scans (on-source integrations, typically 90 s each) were recorded on  $\zeta^1$  UMa each night, with a similar number of scans on  $\gamma$  UMa. We deleted 12 channels at the blue end ( $\lambda < 520$  nm) due to low signal-to-noise ratio. We also removed a small number of channels with bad detectors, as well as the channel contaminated by the HeNe delay-line metrology laser. Typically, each scan produced measurements of  $V^2$  at  $\approx 50$  spatial frequencies. Measuring  $\phi_{cl}$  at a given wavelength requires valid data in the corresponding channel from all three baselines. With this requirement, the typical scan produced 15 measurements of  $\phi_{cl}$ .

For the images presented here, a single calibration factor for  $V^2$  was derived from the calibrator data for each channel, baseline, and night independently. For  $\phi_{cl}$ , a low-order polynomial versus time was fitted. These calibrations used all the calibrators observed during a given night. We are developing more sophisticated calibration methods based on procedures used for the Mark III interferometer (Shao *et al.* 1988; Mozurkewich *et al.* 1991; Armstrong *et al.* 1992).

The uncertainties in the resulting  $V^2$  and  $\phi_{cl}$  are dominated by calibration uncertainties: the formal errors are  $\sim \pm 2\%$  for  $V^2$  and  $\sim \pm 0.5^\circ$  for  $\phi_{cl}$ , but the calibration uncertainties are  $\sim \pm 10\%$  for  $V^2$  and  $\sim \pm 2^\circ$  for  $\phi_{cl}$ . The greatest effect of these uncertainties is on the magnitude difference  $\Delta m$ ; the separations and position angles of the binary components are determined primarily by the location of the maxima and minima of  $V^2$  in the  $(u, v)$  plane, which are only weakly dependent on the calibration.

Figure 1 shows the E-W  $V^2$  data and the  $\phi_{cl}$  data for one of the May 1 scans. The sinusoidal variation of  $V^2$  with increasing wavelength (i.e., decreasing  $(u, v)$  spacing) shows that the binary is clearly resolved on this baseline. The change in  $\phi_{cl}$  of nearly  $180^\circ$  at the wavelength of the minimum in  $V^2$  indicates that the two components of the binary are of nearly equal brightness.

Because the components of  $\zeta^1$  UMa are very similar (Petrie 1939; Fehrenbach & Prevot 1961; Hummel *et al.* 1995), the image structure is wavelength independent, and one can treat the spectral channels as separate  $(u, v)$  samples of a single image. The quality of such a *multichannel optical aperture synthesis* image is much better than that of a single-channel image, since the factor of  $\sim 1.6$  in wave number range across our observed band expands the spatial frequency coverage by the same factor. The orbital period is  $20^d.54$ , so the orbital motion is small during one night. For that reason, we treat all of a given night's scans together, which makes an additional significant improvement in  $(u, v)$  coverage. Figure 2 shows the  $(u, v)$  coverage for the four scans taken on May 1 treated as a single  $(u, v)$  data set.

We used the Astronomical Image Processing System (AIPS) to make one image from the data for each night. For this purpose, we constructed complex visibilities for each baseline and spectral channel by assigning  $(V^2)^{1/2}$  to the visibility amplitudes and zero to two of the visibility phases. We then assigned the calibrated  $\phi_{cl}$  to the phase of the vis-

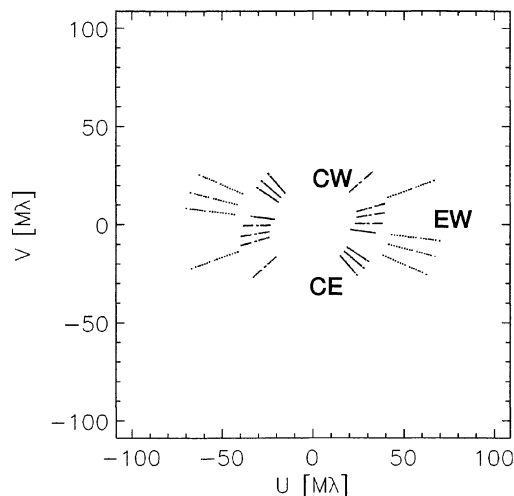


FIG. 2. Spatial frequency coverage for the binary Mizar A on 1996 May 1 with the center, east, and west (“C,” “E,” “W”) elements of the astrometric sub-array of the NPOI. Each baseline produces data from 32 spectral channels and thus results in a ray in the  $(u, v)$  diagram. Four scans of  $(u, v)$  data are shown here, so each baseline produces four rays. The longest  $(u, v)$  spacings are from the east-west (“EW”) baseline. “CW” (upper four rays) and “CE” (lower four rays) indicate data from the two shorter baselines.

ibility on the E-W baseline. This procedure produced a set of 125 to 180 visibilities (depending on the number of scans and of available  $\phi_{cl}$  measurements) from which to generate an image for each night. Standard phase self-calibration methods employed in AIPS readjust the baseline phases while keeping  $\phi_{cl}$  constant. We processed the data with uniform weighting and a cell size of 1 mas, and produced  $256 \times 256$  pixel maps. For the May 1 data, the resulting synthesized beam was  $5.3 \times 1.7$  mas at position angle  $6^\circ$ . This synthesized beam size was typical for all seven nights of observation.

We CLEANed each image, used the CLEAN components as a model for self-calibrating the phases, and re-imaged. The resulting image for the May 1 data, after a few iterations, is shown in Fig. 3. The dynamic range (peak to rms) of this image is  $>100:1$ . Multichannel optical aperture synthesis images for the other six nights, produced in a similar manner to the May 1 image, are shown in Fig. 4. The binary is clearly resolved in all seven images, and the relative motion of the components is evident.

We fitted Gaussian intensity profiles to the images to determine their relative positions. Figure 5 shows these relative positions from the seven nights of observation, as well as the visual orbit (semimajor axis  $a=9.6$  mas, period  $P=20^d.54$ ) determined with the Mark III optical interferometer (Hummel *et al.* 1995). The measured NPOI positions are connected by lines to the positions predicted from the Mark III orbit. The uncertainty ellipses are one-fifth the FWHM of the synthesized beam, a standard criterion used in radio VLBI imaging. The agreement with the Mark III orbit is good, but shows slight systematic differences, which may result from a gap in orbital phase coverage in the Mark III data.

We also note that the shape of the  $\phi_{cl}(\lambda)$  curve and the size of the jump in  $\phi_{cl}$  are sensitive indicators of  $\Delta m$ . For  $\Delta m=0$ ,  $\phi_{cl}(\lambda)$  is a step function of amplitude  $180^\circ$ , with

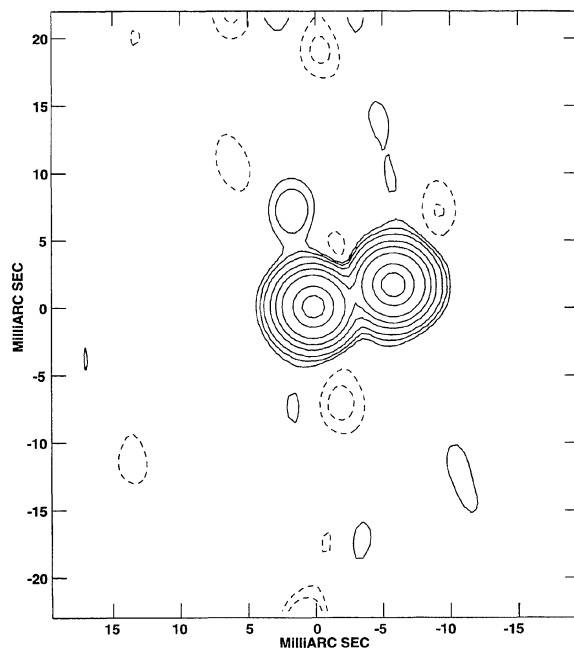


FIG. 3. Image of Mizar A from 1996 May 1. The coordinates are offsets in milliarcseconds between the components. Contour levels are  $-1\%$ ,  $-0.5\%$ ,  $0.5\%$ ,  $1\%$ ,  $2\%$ ,  $5\%$ ,  $10\%$ ,  $20\%$ ,  $50\%$ , and  $80\%$  of the peak flux. Both stars have angular diameters  $\approx 0.8$  mas, and thus are unresolved in these images. The restoring beam was a circular Gaussian of 3 mas diameter (FWHM).

the step at the wavelength of the minimum of the triple amplitude. (For the scan shown in Fig. 1, this occurs at the minimum of  $V^2$  for the EW baseline.) For  $\Delta m \neq 0$ , the size of the jump is less than  $180^\circ$ , and the corners of the step function become rounded. For these data, we have determined a preliminary value for  $\Delta m$  of  $0^m.01 \pm 0^m.01$ , in agreement with earlier estimates that  $\Delta m$  is close to zero (Petrie 1939; Fehrenbach & Prevot 1961; Hummel *et al.* 1995). Our measurement of  $\Delta m$  applies near  $\lambda 700$  nm, where we see the jump in  $\phi_{cl}$ . Since the two components of  $\zeta^1$  UMa are very similar,  $\Delta m$  should be close to zero across the entire band, but measuring  $\Delta m$  as a function of  $\lambda$  requires more data.

The images generated with AIPS, however, show  $\Delta m$  values of up to  $0^m.4$ ; only the May 1 image (Fig. 1) has  $\Delta m < 0^m.1$ . The departures of  $\Delta m$  from zero are probably an artifact of our preliminary calibration of  $V^2$ , which can be biased by calibration errors. The shape of the  $\phi_{cl}(\lambda)$  curve and the size of the jump are much less sensitive to calibration effects.

## 4. DISCUSSION

### 4.1 Broadband Multichannel Data

The images shown here, with a spatial resolution of  $\approx 3$  mas and generated from five to eight minutes of data each, show the power of broadband multichannel optical interferometry. Simultaneous multichannel observations over a broad band produce data at a wide range of spatial frequencies even with only three baselines, providing a dramatic improvement in  $(u, v)$  coverage over that of a monochromatic three-element array (e.g., Baldwin *et al.* 1996). Optical

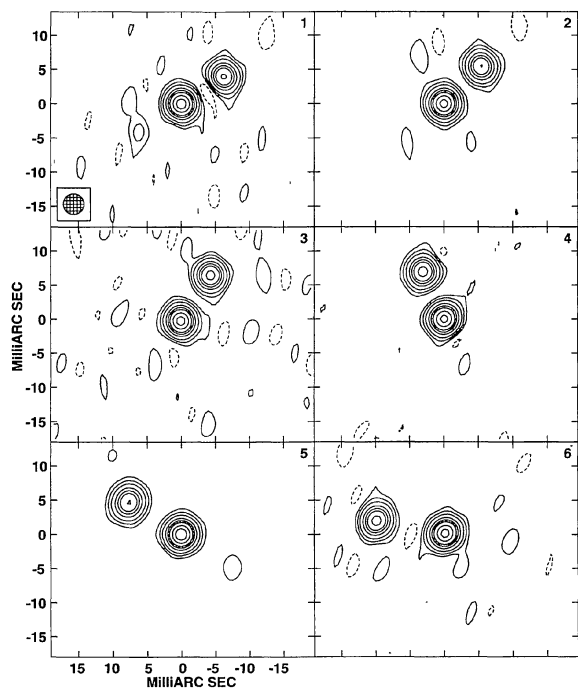


FIG. 4. Images of Mizar A on 1996 May 2, 3, 4, 29, and June 1 and 4 (panels 1–6 respectively). Contour levels are  $-2\%$ ,  $2\%$ ,  $5\%$ ,  $10\%$ ,  $20\%$ ,  $30\%$ ,  $40\%$ ,  $60\%$ , and  $80\%$  of the peak. The 3 mas (FWHM) circular Gaussian restoring beam is shown in panel 1.

interferometers can perform well over a wide wavelength range, while radio astronomical receivers have been limited for historical reasons to a number of narrow discrete bands at wavelengths spaced by factors of roughly two.

Future optical interferometric imaging will continue to depend on large total bandwidths to obtain good  $(u, v)$  coverage. For a number of practical reasons, such as the fact that low-noise coherent optical amplification is not possible, the maximum number of elements in an optical interferometer in the foreseeable future is less than ten. The imaging sub-array of the NPOI, with six elements when complete, will have 15 baselines, as compared with the 351 baselines of the VLA. However, each of the NPOI baselines will take data in 32 channels spanning  $\lambda\lambda$  450–850 nm, thereby expanding its  $(u, v)$  coverage by nearly a factor of two and increasing the number of spatial frequencies to 480. For objects in which the image structure is not independent of wavelength, the analysis must generate images in an  $(\alpha, \delta, \lambda)$  cube rather than in  $(\alpha, \delta)$  alone, but the advantage of a large number and range of spatial frequencies is maintained.

#### 4.2 Vacuum Delay Lines

The vacuum delay lines of the NPOI are crucial for obtaining data over such a wide band, particularly for extending the band to the blue. The greatest part by far of the differences in path length from a star to the interferometer apertures is in vacuum, above the Earth's atmosphere. In the interferometer, these vacuum path length differences can be

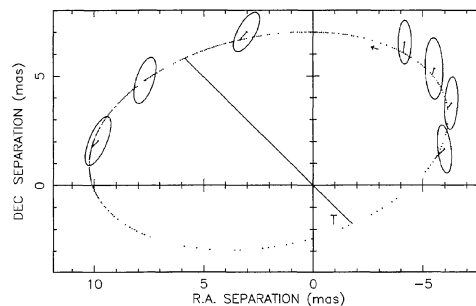


FIG. 5. Binary separations and uncertainty ellipses as obtained from the NPOI data, superposed on the orbit of Hummel *et al.* (1995) from Mark III optical interferometer data. The separations are from fits to the images in Figs. 3 and 4. The ellipses are one fifth of the synthesized beam, a standard VLBI indication of the uncertainty. The measured separations are connected by lines to the separations predicted from the Mark III orbit. The major axis of the orbit is shown, with “T” marking the periastron. The spacing of the dots along the orbit corresponds to  $P/360$ , where  $P=20^d.54$ . A small arrow indicates the sense of the orbital motion.

compensated in vacuum or in air. If they are compensated in air, additional dispersive optics may be needed.

When the vacuum path length differences are compensated with vacuum delay lines, the only remaining differences in air path lengths between beams are due to atmospheric turbulence, so that fringe smearing due to the variation in longitudinal dispersion across a spectral channel or across the observed band is reduced to manageable proportions.

If one used air delay lines but no dispersion-correcting optics, and if  $n(\sigma) - 1$  of air varied only linearly with the wave number  $\sigma$ , one could eliminate the variation of fringe phase with wavelength by suitably adjusting the delay lines. But because of the higher-order terms in  $n(\sigma) - 1$ , which become significant in the blue half of the visual band, eliminating the variation of phase with wavelength in this way is not possible. As an example, for 10 m of air path mismatch between beams, setting the delay lines to minimize the variation of fringe phase still leaves  $>170$  radians of variation within the  $\lambda\lambda$  450–850 nm band and more than 5 radians of variation within most of the 32 individual channels of the NPOI spectrometers.

For relatively short baselines, one can use air delay lines and compensate for the atmospheric dispersion with glass. With the appropriate amount of a typical glass such as BK7 in one interferometer beam compensating for 10 m of air in the other beam, the residual variation of fringe phase across the  $\lambda\lambda$  450–850 nm band is  $\sim 0.3$  radian. But for baselines of 100 m or more, and the corresponding air path mismatches, the residual phase variations after correction are still severe. Even the variation over a 10 nm spectral channel is as large as 0.25 wave, large enough to lead to greatly reduced fringe visibilities.

The large total bandwidth of the NPOI, and therefore the use of vacuum delay lines, was originally driven by the need for milliarcsecond astrometric accuracy. Using a large bandwidth enables us to measure the variation of fringe phase with wavelength, estimate the air path mismatch from this variation, and remove the atmospheric contribution to the delay. The remaining geometric delay is the fundamental as-

trometric datum for an interferometer. The results presented here show the utility of large bandwidths for imaging as well.

#### 4.3 New Analysis Techniques

In radio interferometry, the fundamental data are the complex visibilities  $Ve^{i\phi}$  from pairs of elements. At optical wavelengths, however, the phase of the complex visibility is completely dominated by atmospheric fluctuations, which have a timescale of  $\sim 10$  ms for one-radian fluctuations; thus the phase carries no information about source structure. In addition, the obvious visibility amplitude estimator  $V = (C/N)\langle X^2 + Y^2 \rangle^{1/2}$  [where  $C$  is the normalization factor in Eq. (1)] is biased, since  $\langle X^2 + Y^2 \rangle$  is nonzero (even for zero visibility) due to detector noise (Tango & Twiss 1980), and this bias is a function of  $V$  itself.

The closure phase, however, is free of atmospheric effects, and the  $V^2$  estimator of Eq. (1) is unbiased. For these reasons, the fundamental data for optical interferometric imaging are the  $V^2$  from the interferometer elements taken in pairs and the  $\phi_{\text{cl}}$  for the elements taken in triples. In cases where the visibility on only one of the three baselines of a triple is small, the amplitude of the triple product,  $V_1 V_2 V_3$ , will have a higher signal-to-noise ratio than  $V^2$  for that baseline.

Our results demonstrate the need for analysis techniques that are suited to  $V^2$  and  $\phi_{\text{cl}}$  data. We used the standard radio-interferometric techniques for our images, as did Baldwin *et al.* (1996) for their Capella images, by using the square root of  $V^2$  and by assigning  $\phi_{\text{cl}}$  to one of the baselines. But using these techniques has two disadvantages. One is that  $(V^2)^{1/2}$  is biased: it is always positive, but the measured  $V^2$  may be negative due to noise in  $X$  and  $Y$ . (This bias does not appear to be the cause of the non-zero  $\Delta m$  in our images, however.) The other is that we cannot adjust the relative weights of the  $\phi_{\text{cl}}$  and the  $V^2$  data, since they are

treated together as a complex visibility. Adjusting these relative weights is desirable, since in general they have different signal-to-noise ratios. In the case of our data, the shape of the jump in  $\phi_{\text{cl}}$  is the more sensitive indicator of  $\Delta m$ .

#### 5. CONCLUSION

We have presented the first images from the Navy Prototype Optical Interferometer (NPOI). Multichannel observations over a large total bandwidth provided broad  $(u, v)$  coverage even though we used only three baselines. The vacuum delay lines of the NPOI make it possible to avoid the effects of longitudinal dispersion over a large band. We processed the data with standard radio-interferometry techniques to produce our images. However, the fundamental observables of optical interferometry,  $V^2$  and  $\phi_{\text{cl}}$ , are different from the complex visibilities  $Ve^{i\phi}$  of radio interferometry. Analysis techniques that are more appropriate to the optical interferometry case are clearly needed.

The resolution of  $\approx 3$  mas in our images of the 20<sup>d</sup>54 spectroscopic binary  $\zeta^1$  UMa (Mizar A) is the highest ever attained in an image at visual wavelengths, and exceeds by a factor  $\sim 2-3$  the best resolution *theoretically* obtainable by the largest current monolithic optical telescopes. The separations and position angles of the components of Mizar A in our images show good agreement with the 9.6 mas orbit measured with the Mark III optical interferometer on Mt. Wilson (Hummel *et al.* 1995), but show small systematic differences with the predictions from the Mark III orbit. The differences may be due to a gap in the orbital phase coverage in the Mark III data. The closure phase data are very sensitive to  $\Delta m$ ; our preliminary estimate is that  $\Delta m \approx 0^{\text{m}}01 \pm 0^{\text{m}}01$ .

This research was funded by the Office of Naval Research and the Oceanographer of the Navy.

#### REFERENCES

- Anderson, J. A. 1920, ApJ, 51, 263  
 Armstrong, J. T., *et al.* 1997, ApJ (accepted)  
 Armstrong, J. T., *et al.* 1992, AJ, 104, 241  
 Baldwin, J. E., *et al.* 1996, A&A, 306, L13  
 Brown, R. H., Davis, J., & Allen, L. R. 1974, MNRAS, 167, 121  
 Fehrenbach, C., & Prevot, L. 1961, J. Obs., 44, 83  
 Hummel, C. A., Armstrong, J. T., Buscher, D. F., Mozurkewich, D., Quirrenbach, A., & Vivekanand, M. 1995, AJ, 110, 376  
 Hummel, C. A., *et al.* 1994, AJ, 108, 326  
 Hutter, D. J., *et al.* 1989, ApJ, 340, 1103  
 Jennison, R. C. 1958, MNRAS, 118, 276  
 Johnson, M. A., Betz, A. L., & Townes, C. H. 1974, Phys. Rev. Lett., 33, 1617  
 Labeyrie, A. 1975, ApJ, 196, L71  
 Michelson, A. A., & Pease, F. G. 1921, ApJ, 53, 249  
 Mozurkewich, D., *et al.* 1991, AJ, 101, 2207  
 Mozurkewich, D., *et al.* 1997, in preparation  
 Petrie, R. M. 1939, PubDAO, 7, 205  
 Shao, M., *et al.* 1988, A&A, 193, 357  
 Shao, M., & Staelin, D. H. 1977, J. Opt. Soc. Am., 67, 81  
 Tango, W. J., & Twiss, R. Q. 1980, Prog. Opt., 17, 241